Experimental Mechanics (2008) 48:421–433
DOI 10.1007/s11340-007-9094-0

Identification of Mechanical Material Behavior Through Inverse Modeling and DIC

S. Cooreman · D. Lecompte · H. Sol · J. Vantomme · D. Debruyne

Received: 23 April 2007 / Accepted: 4 October 2007 / Published online: 22 November 2007

Abstract Inverse methods offer a powerful tool for the identification of the elasto-plastic material parameters. One of the advantages with respect to classical material testing is the fact that those inverse methods are able to deal with heterogeneous deformation fields. The basic principle of the inverse method that is presented in this paper, is the comparison between experimentally measured strain fields and those computed by the finite element (FE) method. The unknown material parameters in the FE model are iteratively tuned so as to match the experimentally measured and the numerically computed strain fields as closely as possible. This paper describes the application of an inverse method for the identification of the hardening behavior and the yield locus of DC06 steel, based on a biaxial tensile test on a perforated cruciform specimen. The hardening behavior is described by a Swift type hardening law and the yield locus is modeled with a Hill 1948 yield surface.

Keywords Inverse modeling · FEM · Elasto-plastic material parameters · Heterogeneous deformation fields · Swift type hardening law · Hill 1948 yield surface · Digital image correlation

S. Cooreman (✉, SEM member) · D. Debruyne
Department of Mechanical Engineering,
Technical University KaHo Sint-Lieven,
Gebroeders Desmetstraat 1, 9000 Ghent, Belgium
e-mail: Steven.Cooreman@kahosl.be

D. Debruyne
e-mail: Dimitri.Debruyne@kahosl.be

D. Lecompte, (SEM member) · J. Vantomme
Department of Materials and Construction,
Royal Military Academy, Avenue de la Renaissance 30,
1000 Brussels, Belgium

D. Lecompte
e-mail: DavidLecompte@rma.ac.be

J. Vantomme
e-mail: john.vantomme@rma.ac.be

H. Sol, (SEM member)
Department of Mechanics of Materials and Constructions,
Vrije Universiteit Brussel, Pleinlaan 2,
1050 Brussels, Belgium
e-mail: hugos@vub.ac.be

Introduction

Finite element (FE) simulations are more and more applied in industrial practice for the development and the optimization of metal forming operations to reduce the length and the cost of the "trial and error"- phase. In the case of metal forming, a good knowledge of the elasto-plastic material properties is of the utmost importance in order to perform a sufficiently accurate simulation and to obtain reliable results. In many cases it can be a daunting task to characterize the mechanical behaviour of the material completely, especially when thin sheet specimens are considered that exhibit a substantial anisotropy.

In the past, several tests have been developed to characterize the deformation behaviour of materials: tensile tests [1], compression tests, torsion tests, etc. The deformation fields which are generated during these standard tests are usually homogeneous and do not resemble the complex heterogeneous deformation fields which occur during real metal forming operations.

In general, commercial FE packages implement phenomenological models, with a limited number of unknown parameters, to describe the elasto-plastic material behaviour. However, it should be noted that the validity of those phenomenological models is limited to situations that are comparable to the range of experiments on which they are based. Interpolation between measured data is allowable, but extrapolation is certainly not [2]. As a result, the material behaviour, obtained with these standard tests, is an approximation that in many cases proves insufficient to simulate complex forming operations reliably. This will be discussed in more detail in "Inverse Methods".

To overcome these problems, some authors [3–10] have performed experiments leading to non-uniform stress and strain fields, i.e. by applying complex loading conditions or by using non-conventional specimen geometries. This results in a more complete and realistic description of the material behavior. Then the unknown material parameters are determined by means of a so-called inverse method, i.e. by iteratively minimizing the discrepancy between experimentally measured and numerically computed quantities.

In this paper, a FE based inverse method (see "Inverse Methods") is applied for the characterization of the hardening behavior and the yield locus of DC06 steel, based on a biaxial tensile test on a perforated cruciform specimen. The hardening behavior and the yield locus are described by a Swift type hardening law and a Hill 1948 yield surface respectively. A Gauss–Newton algorithm is applied to minimize the discrepancy between the experimentally measured and the numerically computed strain fields. A similar approach has already been successfully applied for the identification of the 4 in-plane elastic constants of an orthotropic composite material [11].

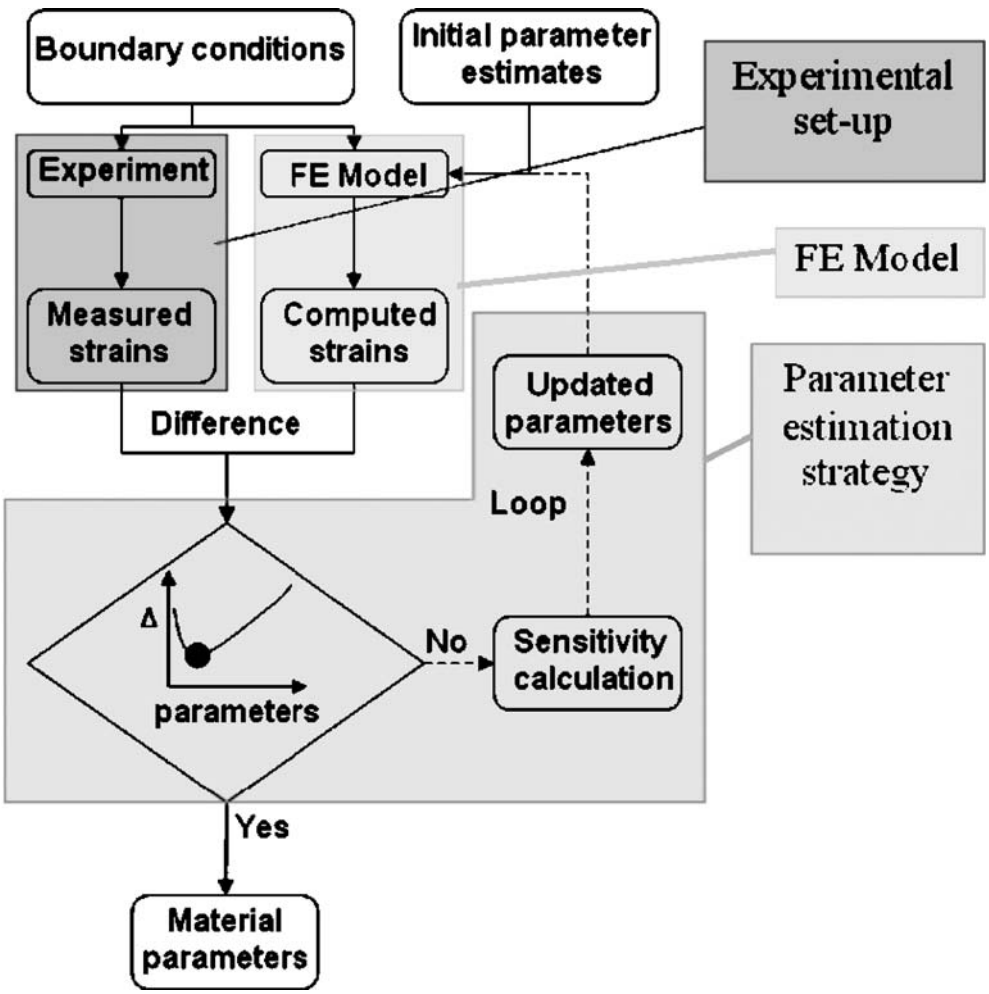

Fig. 1 Flow-chart of the inverse method for material parameter identification

Inverse Methods

Basic Principles

The main goal of an inverse method is to identify a selected set of unknown parameters in a numerical model. The unknown parameters are determined iteratively by minimizing a cost function which expresses the discrepancy between the experimental and the computed response of the physical system under study, e.g. by comparing displacement fields, strain fields, resonant frequencies, etc. In this paper, strain fields are selected as the observation quantity. These heterogeneous strain fields are determined by means of the digital image correlation (DIC) technique. DIC allows, in principle, to measure arbitrary complex (heterogeneous) displacement fields with relative ease [12–14]. Performing some extra calculations on the displacement field yields the strain field. The numerical strain fields are computed with a FE model. The a priori unknown material parameters in the FE model are iteratively updated in such a way that the computed strain fields match the measured fields as closely as possible. Figure 1 shows a flow-chart of the applied inverse method.

An alternative to the above described approach is the virtual fields method [15–17]. As the name of the method suggests, this approach consists of minimizing the difference between the internal and external virtual work of the system by optimizing the elasto-plastic material parameters. This method has two major advantages compared to the FE based inverse method: first, no time-consuming FE computations are required. Second, it is not sensitive to the distribution of the loadings if suitable virtual fields are used. However, since the strain field measurements are only available at the surface of the specimen, it is necessary to make some assumptions concerning the strain field inside the solid. Another drawback is the fact that, until now, no specific rules for the choice of the virtual fields are available in case of elasto-plasticity [10].

Advantages of Inverse Methods

Where standard material tests such as tensile tests and compression tests require uniform stress and strain fields, inverse methods can cope with heterogeneous strain fields. Thus, inverse methods allow to identify the unknown material parameters based on complex material tests, like a biaxial tensile test on a perforated

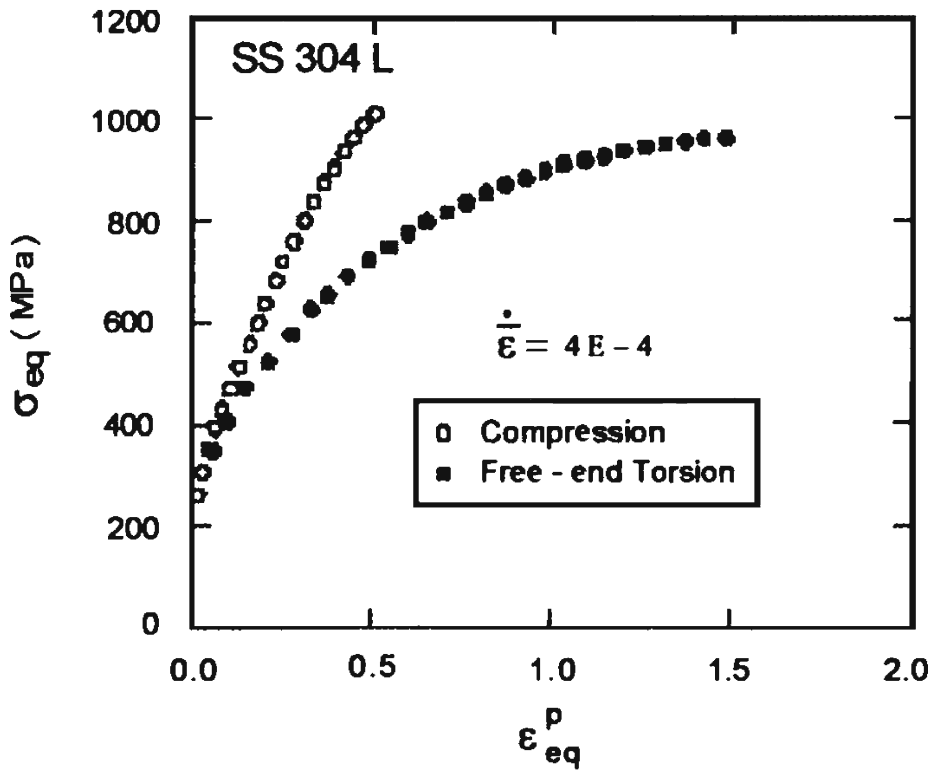

Fig. 2 Experimental data deduced from compression and free-end torsion tests: 304L stainless steel (from Miller and Mc Dowell [26])

cruciform specimen. Heterogeneous deformation fields offer many advantages as compared to homogeneous fields. Heterogeneous strain fields provide much more information and, hence, allow the simultaneous identification of several material parameters. This observation will be illustrated by experimental results further on in this article. Heterogeneous fields also allow the identification of more complex material models with more model parameters.

Another advantage involves the strain path dependency of many metals. Plastic deformation of metals is strain path dependent due to the anisotropic texture which develops or changes during plastic deformation or which was already present in the material due to previous deformation processes, e.g. cold rolling. Widely used material models in industry, such as the von Mises yield surface and Hill's 1948 yield surface, are not able to accurately describe this strain path dependency. This is shown in Fig. 2: this figure plots the von Mises equivalent stress versus the von Mises equivalent strain for experimental data obtained from free-end torsion tests and compression tests for a SS304L steel. It should be noted that the hardening curves obtained from two different material tests do not coincide at all. Thus, for this material the von Mises model is not able to accurately describe plastic deformation along two completely different strain paths.

Another example of strain path dependency is shown in Fig. 3. The full, dark curve shows the equivalent stress—equivalent strain curve for a monotonic tensile test on the large (dark) specimen. After a certain amount of straining, a smaller tensile specimen is cut from the large specimen. Then this small specimen is again loaded in tension, however along a direction which differs from the first tensile direction. As one can see, the equivalent stress—equivalent strain curve obtained from the second tensile test (the dashed curve) does not coincide with the full, dark curve. These strain-path changes are usually not considered when performing material tests in industrial practice. However, they are likely to occur in real metal forming operations. As a result, the material parameters obtained from a simple tensile test will perfectly describe the material behavior in that particular test, but may act completely wrong for other types of deformation. This problem can be partly solved by performing complex material

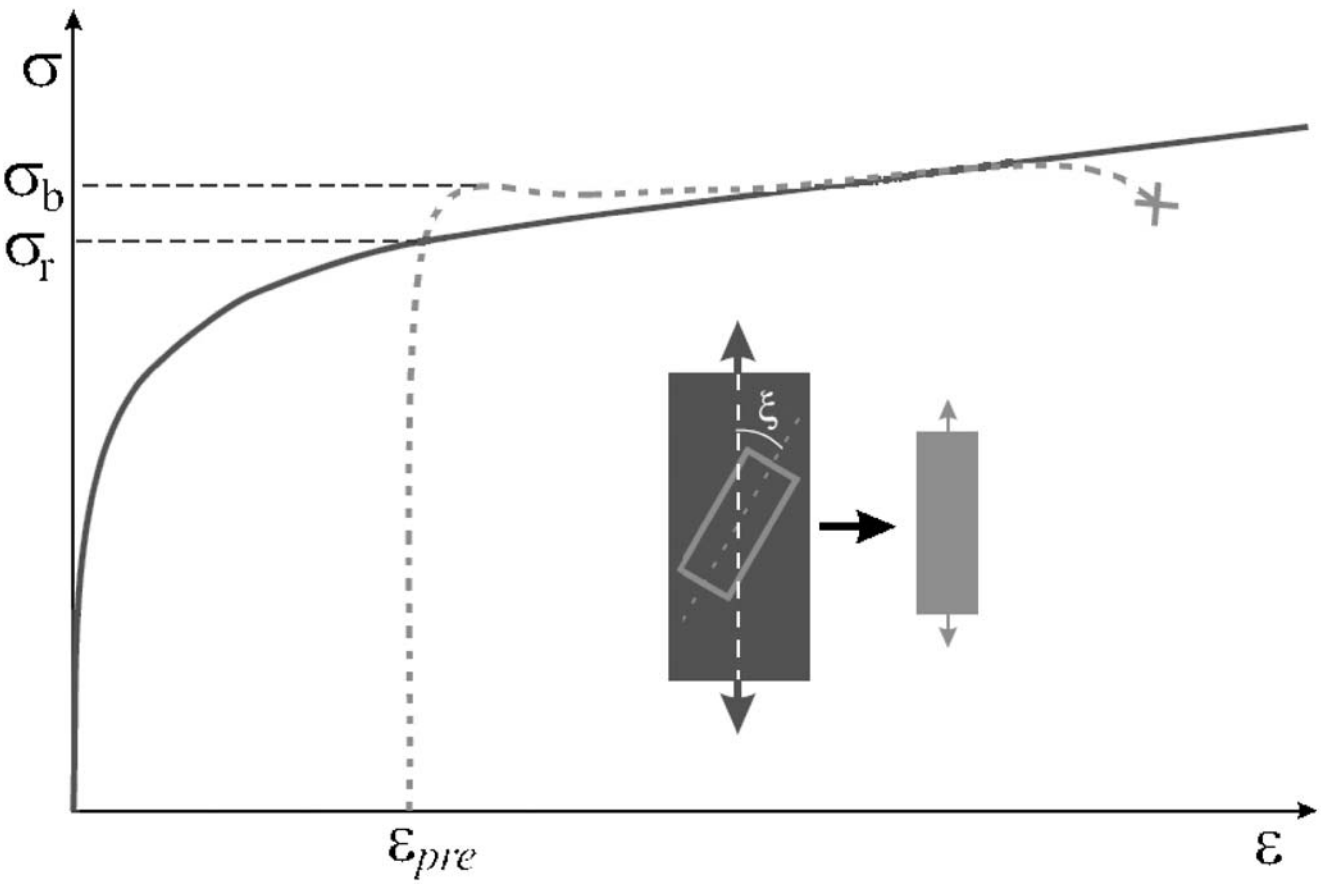

Fig. 3 Influence of strain path changes on the equivalent stress-equivalent strain curve

tests which generate heterogeneous deformation fields, different strain paths and strain path changes: if a simple material model, e.g. Hill's 1948 yield surface with isotropic hardening described by a Swift type hardening law, is identified by means of these complex tests, the obtained material parameters will describe the mechanical material behavior in an average way. As a consequence, the obtained parameters will not allow to perfectly describe one specific way of deformation, e.g. a simple tensile test. The deformation in those complex tests, however, is closer to the deformation in real metal forming operations and as a result the parameters obtained through these complex tests will be more suitable to simulate those metal forming operations.

Experimental Set-Up

Biaxial Tensile Test

The material behavior is determined based on a biaxial tensile test on a perforated cruciform specimen. The selected material is DC06 steel, which has a Young's modulus E of 183 GPa, a Poisson coefficient ν of 0.35, a yield strength σ_0 of $140 MPa$ and a tensile strength of $273 MPa$. The permanent elongation at the tensile strength is about 27%, the permanent elongation after fracture is about 45%. The geometry of the material specimen and the experimental set-up are shown in Figs. 4 and 5 respectively. The specimen has a thickness of 0.8 mm. The specimen's arms are in alignment with the rolling (RD) and transverse direction (TD) of the metal sheet (see Fig. 4). The shaded area indicated in Fig. 4 is the zone in which the experimentally measured strains are compared to the numerical strains (the strains are compared in the Gauss points of the elements of the FE model).

During the biaxial tensile test, the force on the 4 arms is increased up to approximately 4.25 kN. Figure 6 shows a force-displacement plot for one of the arms. The $*$ indicates the load steps which are taken into account during the parameter identification procedure, namely 3.5, 3.76, 4.02, 4.08, 4.14, 4.22 and 4.25 N.

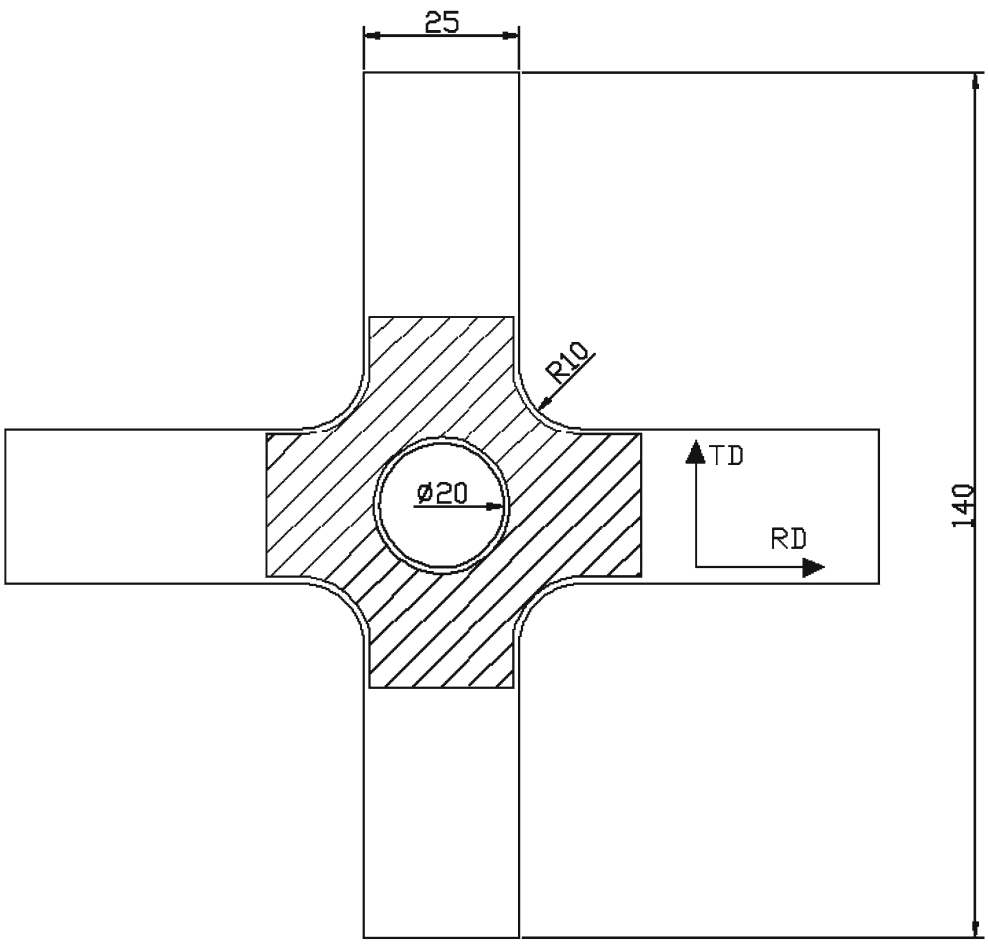

Fig. 4 Geometry of the perforated cruciform specimen

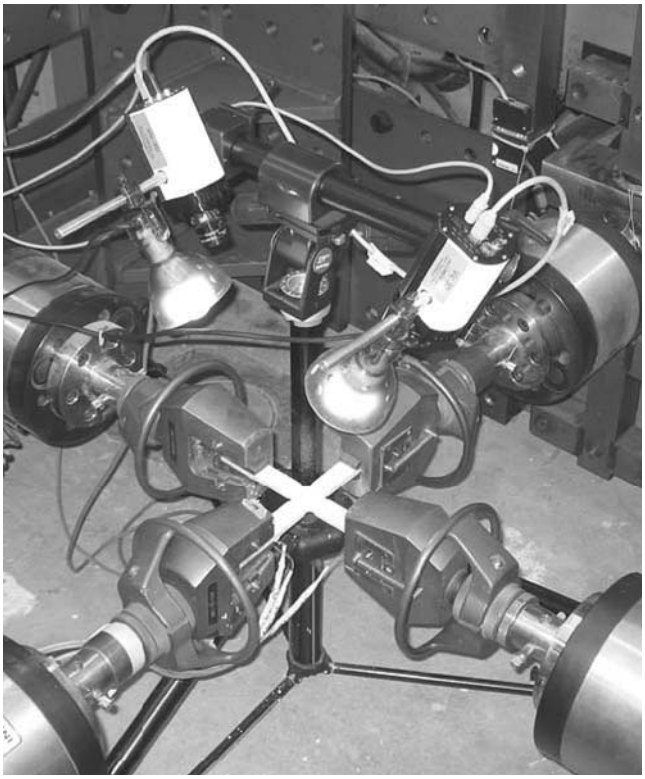

Fig. 5 Experimental set-up: the 4 clamps, the CCD cameras and the cruciform specimen

Strain Field Measurement

As was mentioned in the introduction, the DIC technique is used to measure the strain fields at the top surface of the specimen. Actually, the DIC technique is an optical method to measure displacement fields. However, the strain fields can be computed afterwards based on the measured displacement fields.

Figure 7 shows the working principle of the DIC-system. The system consists of 2 CCD cameras with a resolution of 1,280 by 1,024 pixels. Those cameras take images of the material specimen at the different loading steps. Next, images of the deformed specimen are correlated to an image of the undeformed specimen by means of a sub-pixel algorithm. This correlation procedure goes as follows: a subset of pixels is selected in the undeformed image. Next the correlation software searches for that same subset in the deformed image. Of course, this subset can change size and shape during this correlation process. In order to facilitate this correlation, a random speckle pattern has to be applied on the surface of the specimen. This pattern creates some kind of unique signature for that specific subset. Finally, the displacement field at the surface of the specimen is obtained.

There are two variables which have to be set at the start of the correlation process: the subset size and the step size. The subset size indicates the size of the subset in pixels and can vary from minimum 9×9 pixels to maximum 101×101 pixels. The step size defines how many pixels the subset is shifted in vertical and horizontal direction to calculate the next point. The step size can vary from minimum 1 pixel to maximum half the subset size. The subset size is very important: decreasing the subset size results in a higher

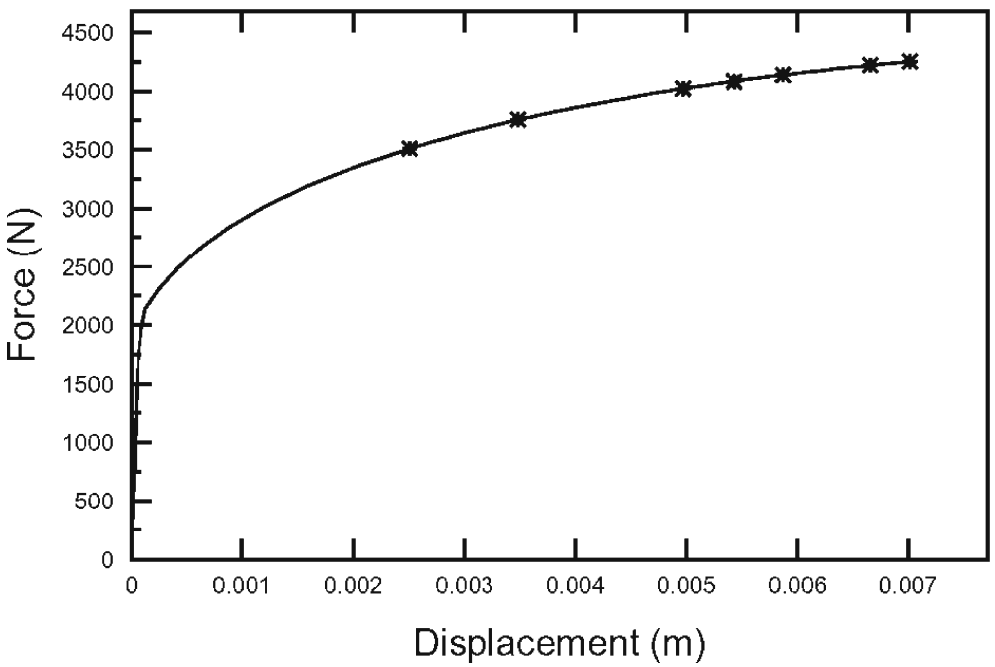

Fig. 6 Force-displacement curve for one of the arms of the biaxial tensile bench

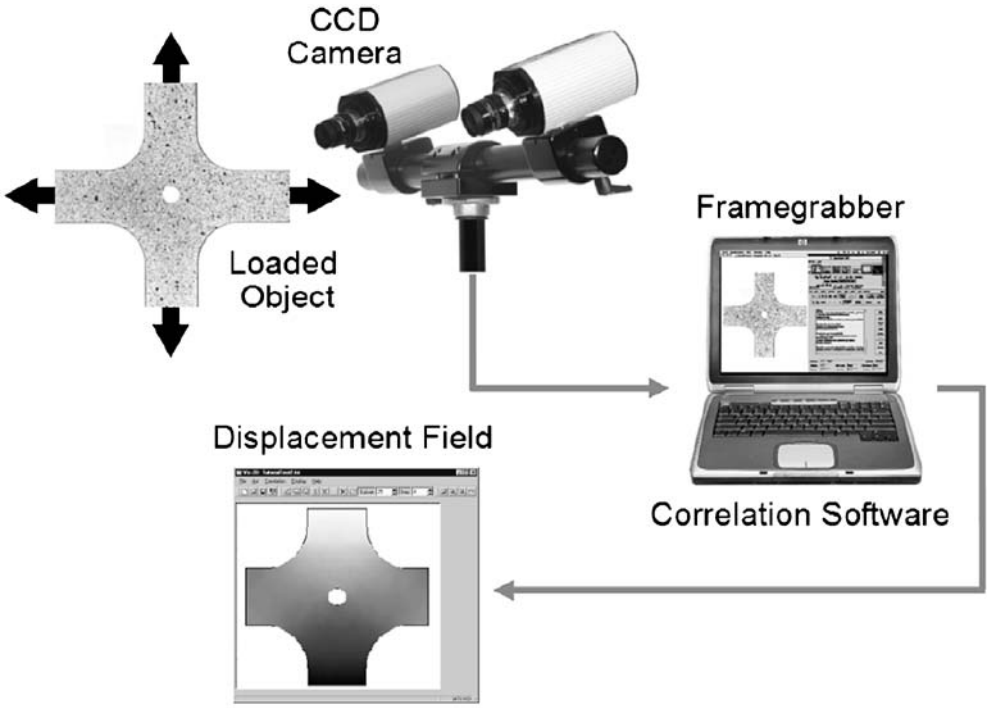

Fig. 7 Working principle of the DIC-system

noise level, increasing the subset size results in more averaging (smoothing of the displacement field). Thus, in regions of homogeneous deformation one may apply a large subset. However, in regions of heterogeneous deformation one should apply a small subset to avoid loss of data. Since the deformation is rather heterogeneous in the neighborhood of the hole, a subset size of 19×19 pixels is applied in this study. The step size only determines the resolution of available displacement data. The smaller the step size, the larger the number of displacement data points and the longer the correlation calculation time. The chosen step size is a compromise between a fair CPU-time and the possibility to treat the displacement data statistically within a given strain window. The step size is set to 5 pixels. The strain field is calculated by numerical differentiation of the displacement field. To this end, a bilinear interpolation function is fitted onto a square region of 5×5 data points (i.e. the strain window size), which is centred on the coordinates of the Gauss-points in the experimental displacement field. The choice of a region containing 5×5 data points is based on a trade-off between too much smoothing when using a larger strain window size and a higher noise influence when using a smaller strain window.

The accuracy of the displacement measurement is between 2% and 5% of the pixel size. In the current setup the resolution is about 0.085 mm/pixel. This results in a maximum measurement error of 4.25 μm. It is much harder to estimate the error on the strain "measurement" since this depends on several factors such as the applied strain window size and the applied smoothing function. The error on the strain "measurement" can be estimated to be of the order of 500 μstrain.

Numerical Model

The numerical strain fields are computed with the commercial FE package Abaqus/Standard [18]. The cruciform specimen is modeled with 1,672 S4R elements (linear shell elements with reduced integration), which is a valid representation since the out-of-plane shear stresses will be negligible. The constitutive model used in the FE model is a hypoelastic-plastic formulation, assuming that the total logarithmic strain rate $\overline{\overline{D}}$ can be additively split into an elastic and a plastic part:

$$\overline{\overline{D}} = \overline{\overline{D}}^{el} + \overline{\overline{D}}^{pl} \tag{1}$$

Moreover an associated flow rule is applied, assuming normality of the plastic strain rate to the yield surface:

$$\overline{\overline{D}}^{pl} = \dot{\lambda} \frac{\partial \Phi}{\partial \overline{\overline{\sigma}}} \tag{2}$$

with $\dot{\lambda}$ the plastic multiplier, Φ the yield surface and $\overline{\overline{\sigma}}$ the Cauchy stress tensor. The material is assumed to be elastically isotropic and plastically orthotropic. Moreover the elastic constants are assumed to be known, namely a Young's modulus E of 183 GPa and a Poisson coefficient ν of 0.35. As was already men-

tioned, the yield surface is described by Hill's 1948 yield criterion:

$$\Phi = F(\sigma_{yy}-\sigma_{zz})^2 + G(\sigma_{zz}-\sigma_{xx})^2 + H(\sigma_{xx}-\sigma_{yy})^2 + 2L\tau_{yz}^2 + 2M\tau_{xz}^2 + 2N\tau_{xy}^2 - \sigma_{eq}^2 = 0 \quad (3)$$

Since we may assume plane stress conditions, Hill's 1948 yield criterion reduces to:

$$(G+H)\sigma_{xx}^2 + (F+H)\sigma_{yy}^2 - 2H\sigma_{xx}\sigma_{yy} + 2N\tau_{xy}^2 - \sigma_{eq}^2 = 0 \quad (4)$$

with σ_{eq} the equivalent stress and $G+H=1$. The hardening behavior is described by a Swift type hardening law:

$$\sigma_{eq} = K\left(\epsilon_0 + \epsilon_{eq}^{pl}\right)^n \quad (5)$$

with K the deformation resistance, ϵ_0 some kind of prestrain, ϵ_{eq}^{pl} the equivalent plastic strain and n the hardening exponent. It should be noted that neither kinematic hardening nor strain rate dependency are considered. Thus a total of 6 material parameters have to be identified: n, K, ϵ_0, F, H and N. The initial parameter values are estimated as: $n=0.3$, $K=600MPa$, $\epsilon_0=0.005$, $F=G=H=0.5$ and $N=1.5$ (i.e. assumption of isotropic behavior).

Updating Procedure

Gauss–Newton Algorithm

Those 6 unknown material parameters are determined in an iterative way by minimizing a cost function $C(\overline{p})$ which expresses the discrepancy between the experimentally "measured" and the numerically computed strain fields. A simple, yet very performant cost function $C(\overline{p})$ is a least squares expression:

$$C(\overline{p}) = \frac{1}{3m}\left(\Sigma_{i=1}^{i=m}\left(\left(\left(\epsilon_{xx}^{exp}\right)_i - \left(\epsilon_{xx}^{num}(\overline{p})\right)_i\right)^2 + \left(\left(\epsilon_{yy}^{exp}\right)_i - \left(\epsilon_{yy}^{num}(\overline{p})\right)_i\right)^2 + \left(\left(\epsilon_{xy}^{exp}\right)_i - \left(\epsilon_{xy}^{num}(\overline{p})\right)_i\right)^2\right)^{\frac{1}{2}} \quad (6)$$

with m the number of geometrical points in which the strains are measured, $(\epsilon_{xx}^{exp})_i$, $(\epsilon_{yy}^{exp})_i$ and $(\epsilon_{xy}^{exp})_i$ the experimentally measured strains, $(\epsilon_{xx}^{num})_i$, $(\epsilon_{yy}^{num})_i$ and $(\epsilon_{xy}^{num})_i$ the numerically computed strains and $\overline{p}$ the column of unknown parameters. It should be noted that only the in-plane strains at the top surface of the specimen can be considered, since only the displacements at the surface of the specimen can be measured. In general, a distinction can be made between zero-order optimization methods, where only cost function evaluations are needed (e.g. Simplex and Genetic algorithms) and first-order optimization methods, which require gradient evaluations of the cost function (e.g. Gauss–Newton and Levenberg–Marquardt). In the case of elasto-plastic material parameter identification, the latter approach seems to be the most efficient since this method requires far less iterations, resulting in less time-consuming elasto-plastic FE simulations. In this paper, a Gauss–Newton update algorithm was applied to minimize the cost function $C(\overline{p})$.

The necessary condition for a cost function to attain its minimum can be expressed by stating that the partial derivatives of this cost function with respect to the unknown material parameters have to be zero:

$$\frac{\partial C(\overline{p})}{\partial p_i} = 0 \quad (7)$$

Since the real cost function is not known, it is locally approximated by a second order Taylor series around the current parameter values (as is shown in Fig. 8):

$$C(\overline{p}) \approx C^*(\overline{p}) = \left[C(\overline{p})\right]_{\overline{p}=\overline{p}^k} + \left[\frac{\partial C(\overline{p})}{\partial p_i}\right]_{\overline{p}=\overline{p}^k}\left(p_i - p_i^k\right) + \frac{1}{2}\left[\frac{\partial^2 C(\overline{p})}{\partial p_i \partial p_j}\right]_{\overline{p}=\overline{p}^k}\left(p_i - p_i^k\right)\left(p_j - p_j^k\right) \quad (8)$$

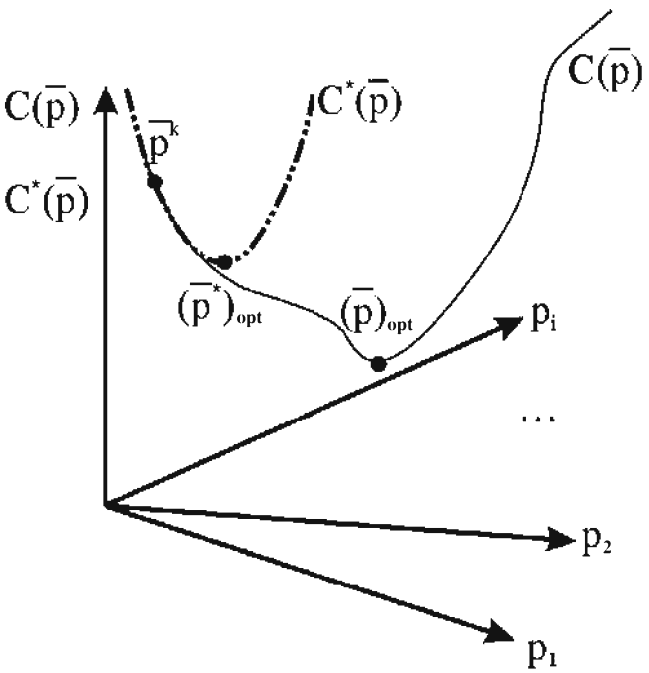

Fig. 8 The real cost function $C(\overline{p})$ is locally approximated by a second order Taylor series $C^*(\overline{p})$ around the current parameter values $\overline{p}^k$

With $C(\overline{p})$ the real cost function, $C^*(\overline{p})$ the local approximation of the real cost function and $\overline{p}^k$ the column of unknown material parameters at iteration step k. Thus, the Gauss–Newton algorithm determines the minimum of the local approximation and that is why it is an iterative procedure. Substituting equation (8) into equation (7) yields the final Gauss–Newton update algorithm:

$$\overline{\Delta p} = \left(\overline{\overline{S^k}}^T . \overline{\overline{S^k}}\right)^{-1} . \overline{\overline{S^k}}^T . \left(\overline{\epsilon^{exp}} - \overline{\epsilon^{num}}\left(\overline{p^k}\right)\right) \tag{9}$$

with $\overline{\Delta p}$ the column of parameter updates, $\overline{\overline{S}}$ the sensitivity matrix, $\overline{\epsilon}^{exp}$ the column of experimentally measured strains and $\overline{\epsilon}^{num}(\overline{p}^k)$ the column of numerically computed strains as a function of the unknown material parameters at iteration step k. The sensitivity matrix $\overline{\overline{S}}$ is defined as:

$$S_{ij} = \frac{\partial \epsilon_i^{num}}{\partial p_j} \tag{10}$$

and expresses the sensitivity of the numerically computed strains with respect to the unknown material parameters.

It should be noted that the Gauss–Newton update algorithm is a local optimizer. Therefore, good initial parameter estimates and an accurate computation of the sensitivity matrix are of the utmost importance for a fast and stable convergence to the global minimum. Bad initial estimates may cause the algorithm to converge to a local minimum and may increase the number of iterations needed to reach the minimum.

Sensitivity Matrix Computation

The sensitivity matrix can be computed in several ways. The most straightforward way is by finite differentiation [19, 20]:

$$\frac{d\,\overline{\epsilon}^{num}}{dp_i} \approx \frac{\Delta\overline{\epsilon}^{num}}{2\Delta p_i} = \frac{\overline{\epsilon}^{num}(p_i + \Delta p_i) - \overline{\epsilon}^{num}(p_i - \Delta p_i)}{2\Delta p_i} \tag{11}$$

with $\Delta p_i = 0.001\,p_i$, a small variation of the parameter value. Usually the above equation is simplified to:

$$\frac{d\,\overline{\epsilon}^{num}}{dp_i} \approx \frac{\Delta\overline{\epsilon}^{num}}{\Delta p_i} = \frac{\overline{\epsilon^{num}}(p_i + \Delta p_i) - \overline{\epsilon}^{num}(p_i)}{\Delta p_i} \tag{12}$$

Finite differentiation requires recomputation of the strains for small variations of each of the parameter values. This is time consuming since the number of necessary FE simulations will increase linearly with the number of unknown material parameters. Two other methods are the adjoint method [21] and direct differentiation [21–23]. Both methods have to be implemented in the FE code, what is not always straightforward when using a commercial FE code. Therefore, our goal is to develop an analytical method for the sensitivity computation. This can be done quite easily in case of linear elastic behavior [11], but becomes much harder in the case of plastic deformation because of the strain path dependency which has to be taken into account. In fact, the following expression has to be computed:

$$\begin{aligned}\frac{d\,\overline{\overline{\epsilon}}}{dp_i} &= \frac{d}{dp_i}\left(\int_S\left(\overline{\overline{D}}\right)\right) = \frac{d}{dp_i}\left(\int_S\left(\overline{\overline{D}}^{el} + \overline{\overline{D}}^{pl}\right)\right)\\ &= \frac{d}{dp_i}\left(\int_S\left(\overline{\overline{D}}^{el}\right)\right) + \frac{d}{dp_i}\left(\int_S\left(\overline{\overline{D}}^{pl}\right)\right)\end{aligned} \tag{13}$$

with $\overline{\overline{\epsilon}}$ the total logarithmic strain and $\overline{\overline{D}}$ the total logarithmic strain rate. If we assume p_i to be one of the plastic material parameters, expression equation (13) can be further elaborated:

$$\begin{aligned}&\frac{d}{dp_i}\left(\int_S\left(\overline{\overline{D}}^{el}\right)\right) + \frac{d}{dp_i}\left(\int_S\left(\overline{\overline{D}}^{pl}\right)\right)\\ &= \overline{\overline{\overline{C}}} : \frac{d\overline{\overline{\sigma}}}{dp_i} + \frac{d}{dp_i}\left(\int_S\left(\dot{\lambda}\frac{\partial\Phi}{\partial\overline{\overline{\sigma}}}\right)\right)\end{aligned} \tag{14}$$

Thus, one also has to take into account the variation of the Cauchy stress (due to geometrical changes, redistribution of the internal forces, etc.) when calculating the sensitivity of the strains with respect to the unknown material parameters. More information on the above described analytical approach can be found in Cooreman et al. [24]. In the present paper, the sensitivity matrix is computed by finite differentiation [equation (12)].

Results

Inverse Methods

Figures 9 and 10 show plots in the σ_{xx}-σ_{yy}-σ_{xy} space of stress states which occur during the biaxial tensile test and which are on the initial yield surface. As one can see, a large part of the initial yield surface is covered, indicating that many different strain paths are represented. As a result, the identified parameters will describe the material behavior in an average way. Figure 11 shows plots of the total logarithmic strain fields and the equivalent plastic strain field at the end of load step 7.

The criterion used to end the iterative process is based on the values of the updates for the different

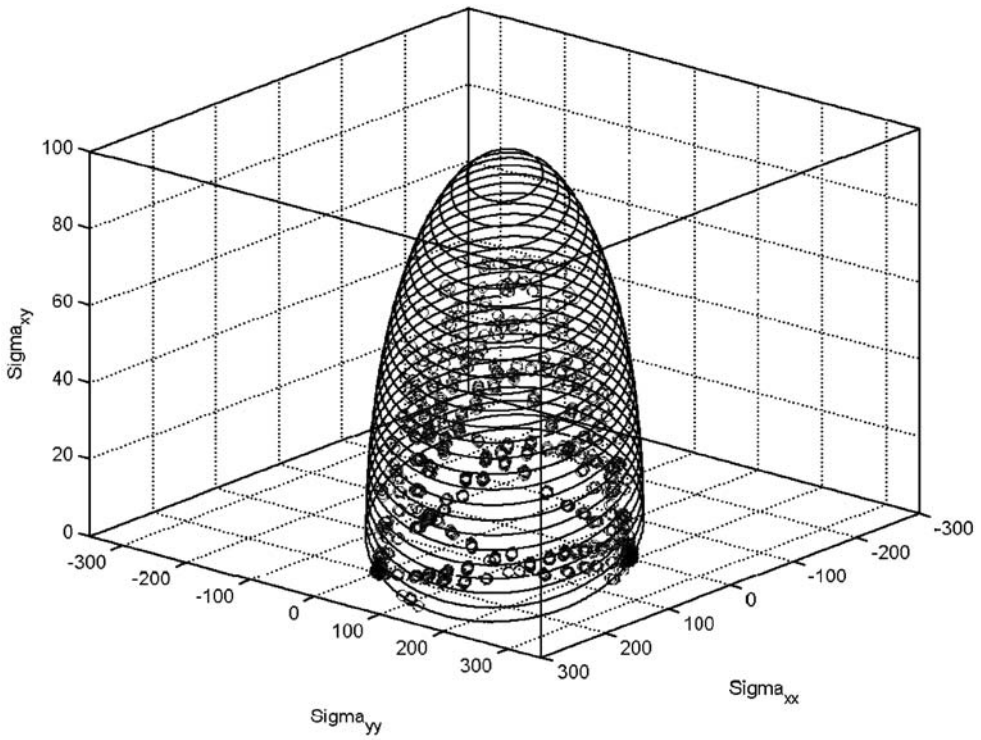

Fig. 9 Plot in σ_{xx}-σ_{yy}-σ_{xy} space of stress states which occur during the biaxial tensile test and which are on the initial yield surface

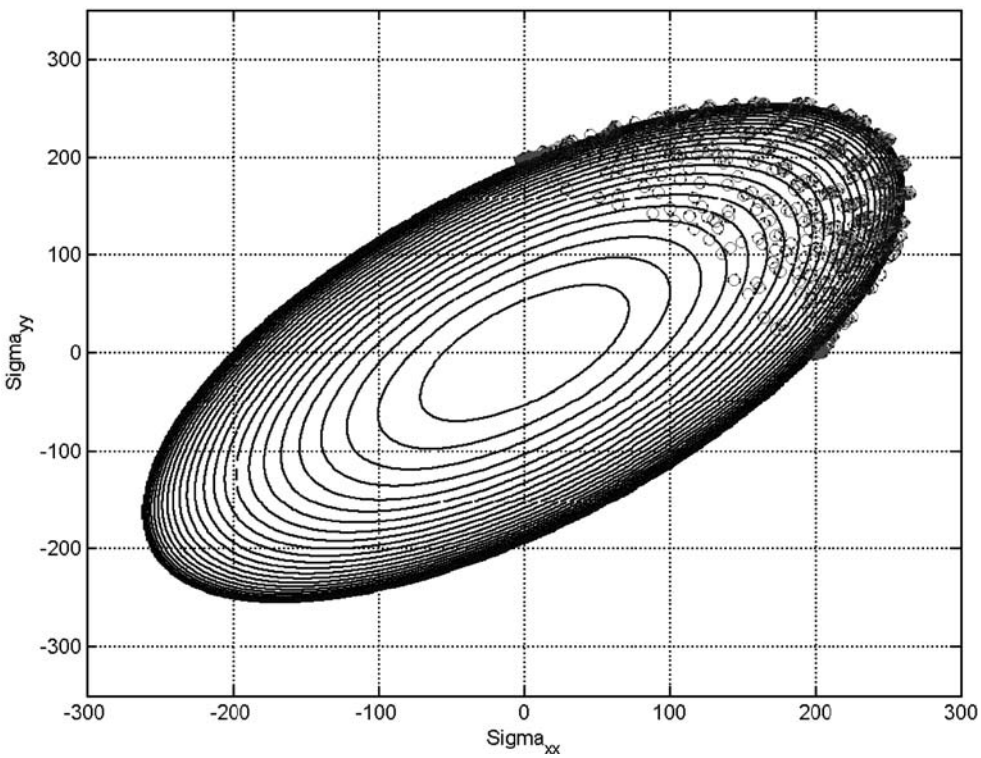

Fig. 10 Plot in σ_{xx}-σ_{yy}-σ_{xy} space of stress states which occur during the biaxial tensile test and which are on the initial yield surface (top view)

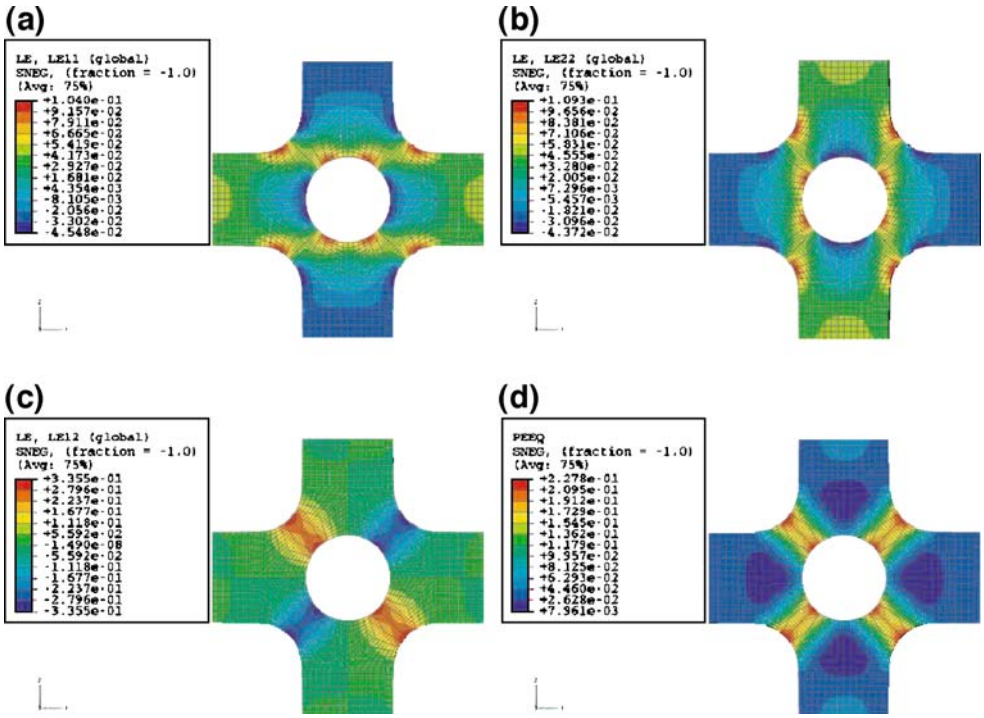

Fig. 11 Plots of the total logarithmic strain fields at the end of load step 7(**a**) ϵ_{11}; (**b**) ϵ_{22}; (**c**) γ_{12} ($= 2\epsilon_{12}$); (**d**) equivalent plastic strain ϵ_{eq}^{pl}

material parameters: when the ratio between the value of the updates and the actual parameter values drops below 0.5%, the routine is stopped. This convergence criterion was reached after 5 iterations. The converged values are summarized in Table 1.

Validation of the Results with Classical, Homogeneous Material Tests

The DC06 steel has been identified by Flores [25] based on the Lankford coefficients and the stress-state fitting. The yield stress and the hardening parameters are determined by uni-axial tensile tests at different angles with respect to the rolling direction, using an offset strain value of 0.2% for the yield stress. As a result the obtained hardening parameters will describe the material hardening in an average way. The parameters of the Hill yield surface are determined in two ways: based on the Lankford coefficients (i.e. the traditional way) and based on stress-state fitting of the yield surface (i.e. a more advanced method). The Lankford coefficients are measured from uni-axial tensile data in the rolling (RD), the transverse (TD) and the 45° direction. The anisotropy coefficient is computed by the ratio of the width and the thickness plastic strain rates. The obtained values are: $r_{0^\circ} = 1.98$, $r_{90^\circ} = 2.56$ and $r_{45^\circ} = 1.67$. Eight experimental tests (tensile tests, plain strain tests and simple shear tests) are performed in order to define the initial yield surface for the yield locus parameter identification by stress-state fitting. As a result, the Hill parameters obtained through stress-state fitting, should again describe the yield surface in a more average way. The identified values of the different parameters are summarized in Table 1.

The results of the inverse method and the classic, homogeneous tests are quite similar, except for the

Table 1 Classical test vs. inverse method

Parameter	Inverse method	Classical test	
ϵ_0	0.00253	0.0063	
K (MPa)	493	500	
n	0.257	0.25	
		Lankford coefficients	Stress-state fitting
F	0.405	0.26	0.495
H	0.633	0.665	0.505
N	1.438	1.27	1.52

prestrain ϵ_0. It can be noted from Table 1 that the values of the Hill parameters obtained by inverse methods are in general closer to the values of the Hill parameters obtained by stress-state fitting. Probably this can be explained by the fact that in case of the inverse method and the stress-state fitting many more different stress-states are available to identify the Hill parameters. In case of the Lankford coefficients, the Hill parameters are determined based on the ratio between the width and thickness plastic strain rate. The parameters obtained through stress-state fitting and inverse modeling will describe the yield surface in a more average way.

The fact that the prestrain ϵ_0 differs so much can probably be explained by the fact that almost no strain data at initial yielding is available. This can be seen from Fig. 6 which plots the force-displacement curve for one of the arms of the biaxial tensile bench. Pictures were only taken at the load steps indicated by a $*$. As one can see those load steps are far beyond the initiation of plastic deformation. For large plastic strains, the value of the prestrain ϵ_0 is less important. Thus, the physical system under consideration, i.e. the 7 load steps, is rather insensitive to the value of ϵ_0. As a result it is hard to determine the prestrain ϵ_0 accurately. Therefore more load steps closer to the initial yield point will be taken into account in future research.

General Conclusions and Future Work

A method has been proposed to simultaneously determine the parameters F, H and N of the Hill yield surface and the parameters ϵ_0, K and n of the Swift type hardening law. The method is based on the inverse modeling of a perforated cruciform specimen under biaxial tension. A least-squares formulation of the difference between the experimental and the numerical strain fields is used along with a Gauss–Newton type optimization algorithm. The proposed method allows the determination of averaged material parameters, based on the high information contents of heterogeneous strain fields. The results are better suited for the simulation of real metal forming processes than results based on classical homogeneous tests like tensile tests.

In the future other material tests will be performed and other material models will be applied. The influence of the number and the spreading of the load steps considered in the identification process will also be studied.

References

1. ASTM (1996) ASTM Standard E8M-96. Standard test methods for tension testing of metallic materials [metric]. In: Annual book of ASTM standards, vol. 03.01. ASTM, Philadelphia, pp 76–96.
2. Boogaard AH (2002) Thermally enhanced forming of aluminium sheet. PhD thesis, Twente University, Twente, The Netherlands.
3. Mahnken R, Stein E (1996) A unified approach for parameter identification of inelastic material models in the frame of the finite element method. Comput Methods Appl Mech Eng 136:225–258.
4. Khalfallah A, BelHadjSalah H, Dogui A (2002) Anisotropic parameter identification using inhomogeneous tensile test. Eur J Mech A Solids 21:927–942.
5. Endelt B, Nielsen KB (2005) General framework for analytical sensitivity analysis for inverse identification of constitutive parameters. In: Proceedings of COMPLAS 2005, 8th international conference on computational plasticity. Barcelona, Spain, 5–7 September.
6. Ghouati O, Gelin JC (1998) Identification of material parameters directly from metal forming processes. J Mater Process Technol 80–81:560–564.
7. Ghouati O, Gelin JC (2001) A finite element-based identification method for complex metallic material behaviour. Comput Mater Sci 21:57–68.
8. Kajberg J, Lindkvist G (2004) Characterization of materials subjected to large strains by inverse modelling based on in-plane displacement fields. Int J Solids Struct 42:3439–3459.
9. Meuwissen M, Oomens C, Baaijens F, Petterson R, Janssen J (1998) Determination of the elasto-plastic properties of aluminium using a mixed numerical-experimental procedure. J Mater Process Technol 75:204–211.
10. Grédiac M, Pierron F (2006) Applying the virtual fields methods to the identification of elasto-plastic constitutive parameters. Int J Plast 22:602–627.
11. Lecompte D, Smits A, Sol H, Vantomme J, Van Hemelrijck D (2007) Mixed numerical-experimental technique for orthotropic parameter identification using biaxial tensile tests on cruciform specimens. Int J Solids Struct 44:1643–1656.
12. Peters WH, Ranson WF (1982) Digital image techniques on experimental stress analysis. Opt Eng 21(3):427–431.
13. Chu TC, Ranson WF, Sutton MA, Peters WH (1985) Applications of digital image correlation techniques to experimental mechanics. Exp Mech 25(3):232–244.
14. Sutton MA, Wolters WJ, Peters WH, Ranson WF, McNeil SR (1983) Determination of displacements using an improved digital correlation method. Image Vis. Comput. 1(3): 133–139.
15. Grédiac M, Toussaint E, Pierron F (2002) Special virtual fields for the direct determination of material parameters with the virtual fields method. 1—Principle and definition. Int J Solids Struct 39:2691–2705.
16. Grédiac M, Toussaint E, Pierron F (2002) Special virtual fields for the direct determination of material parameters with the virtual fields method. 2—Application to in-plane properties. Int J Solids Struct 39:2707–2730.
17. Grédiac M, Toussaint E, Pierron F (2003) Special virtual fields for the direct determination of material parame-

ters with the virtual fields method. 3—Application to the bending rigidities of anisotropic plates. Int J Solids Struct 40:2401–2419.
18. Abaqus Inc. (2006) ABAQUS theory manual, version 6.6. Simulia, Providence.
19. Ghouati O, Gelin JC (1997) An inverse approach for the identification of complex material behaviours. In: Sol H, Oomens CWJ (eds) Material identification using mixed numerical experimental methods. Kluwer Academic Publishers, Dordrecht, pp 93–102.
20. Meuwissen M, Oomens C, Baaijens F, Petterson R, Janssen J (1997) Determination of parameters in elasto-plastic models of aluminium. In: Sol H, Oomens CWJ (eds) Material identification using mixed numerical experimental methods. Kluwer Academic Publishers, Dordrecht, pp 71–80.
21. Grešovnik I (2000) A general purpose computational shell for solving inverse and optimisation problems. PhD thesis, University of Wales.
22. Kleinermann JP (2000) Identification paramétrique et optimalisation des procédés de mise à forme par problems inverses. Doctoral thesis, University of Liège.
23. Ponthot JP, Kleinermann JP (2006) A cascade optimization methodology for automatic parameter identification and shape/process optimization in metal forming simulation. Comput Methods Appl Mech Eng 195:5472–5508.
24. Cooreman S, Lecompte D, Sol H, Vantomme J, Debruyne D (2007) Elasto-plastic material parameter identification by inverse methods: calculation of the sensitivity matrix. Int J Solids Struct 44:4329–4341.
25. Flores P (2005) Development of experimental equipment and identification procedures for sheet metal constitutive laws. PhD thesis, Université de Liège, Liège, Belgium.
26. Miller MP, Mc Dowell DL (1996) Modeling large strain multiaxial effects in FCC polycrystals. Int J Plast 12(7): 875–902